Oxidation of Metals, Vol. 14, No. 2, 1980

Oxidation of Ni–Cr–W Ternary Alloys

S. Espevik,*† R. A. Rapp,* P. L. Daniel,*‡ and J. P. Hirth*

Received September 7, 1978

The oxidation behavior in air at 1000–1250°C of four Ni–Cr–W alloys containing sufficient chromium content (~22 at.% Cr) for protective Cr_2O_3 formation in a binary Ni–Cr alloy is reported. Generally for alloys high in W (10 and 16 at.% W), the rejection of tungsten into the alloy beneath the scale introduced a steep Cr concentration gradient and slower Cr diffusion such that continuous precipitation of Cr_2O_3 internal oxides prevented the formation of a Cr_2O_3 protective scale. The alloy most dilute in W (1.6 at.% W) formed a protective scale at short times with little outer NiO scale, but scale fractures led to internal oxidation and rapid nonprotective kinetics. After an initially rapid oxidation increment to form NiO, the 3 at.% W alloy formed a protective Cr_2O_3 scale with about the same steady-state parabolic kinetics as a binary Ni–30Cr alloy. The effect of ternary W additions on the development of Cr_2O_3 scales on Ni–Cr–W alloys is considered as a ternary analog to Wagner's description of the oxidation of Cu–Pt or Cu–Pd alloys.

KEY WORDS: alloy oxidation; nickel–chromium–tungsten; scale formation; kinetics.

INTRODUCTION

The alloys in current use in the hot section of aircraft turbine engines are nickel- or cobalt-base with a major addition (10 to 20%) of chromium for oxidation and hot-corrosion resistance, aluminum (in the nickel-base alloys) to form the strengthening intermetallic γ' (Ni_3Al), and usually tungsten to provide solid solution strengthening. In turbine service the alloys are protected from severe oxidation by an aluminide diffusion coating which forms a protective Al_2O_3 scale. In less demanding and less critical

*Department of Metallurgical Engineering, The Ohio State University, Columbus, Ohio.
†Former address: Scandinavian Institute of Dental Materials, Oslo, Norway (deceased).
‡Present address: Babcock and Wilcox Research Lab., Alliance, Ohio.

0030-770X/80/0400-0085$03.00/0

applications, Ni-base, W-strenthened superalloys are used in the uncoated condition, in which case oxidation resistance is achieved by a protective Cr_2O_3 scale. While the presence of the refractory metal strengthener is quite necessary for the mechanical properties, the role of tungsten in the oxidation of the alloys has not been previously investigated in detail.

The reaction and effect of the W component in oxidation are expected to be complicated because of several simultaneous possibilities. First, the highest oxide of tungsten (WO_3) melts at a low temperature and exhibits an extremely high vapor pressure as WO_3 molecules, or as multiples of these molecules $(WO)_3)_n$, or as the hydrated trioxide molecules in the presence of water vapor.[1]

Second, if a protective Cr_2O_3 (or Al_2O_3) scale is formed on a multicomponent alloy containing W, then the less stable, lowest oxide WO_2 should not form, but some W ions could nevertheless be dissolved into the protective scale. Although the valence of such ions is uncertain, soluble ions could "dope" the protective scale as an aliovalent (non-three-plus) ion which should affect the defect structure of the scale and the kinetics of oxidation according to the Wagner–Hauffe theory.

The third possible role for W in the presence of Cr_2O_3 scale formation is its rejection (partitioning) from the scale at the metal–scale interface. Then the more noble W component would diffuse inward into the alloy; because of its low intrinsic diffusion coefficient, steep gradients for the components beneath the protective scale would be expected. This rejection of the W component and the steep concentration gradient could cause a "breakaway" or accelerated oxidation phenomenon if the component forming the protective scale became subject to internal oxidation, or if the Cr_2O_3 scale should spall or fracture.

Wagner[2] has examined theoretically an unusual morphological occurrence in the oxidation of Cu–Pt and Cu–Pd alloys. In these alloys, only the copper component forms a stable oxide and the noble metal is rejected at the metal–scale interface and diffuses into the alloy. As an exceptional occurrence, these alloys form Cu_2O both as an external scale and as internal oxide precipitates. The free energy driving force required to form Cu_2O precipitates under a Cu_2O scale is provided by the steep gradient in the noble metal concentration, so that the copper activity is lower immediately beneath the scale than farther into the alloy. Wagner[2] solved the diffusion equation for the oxygen and copper concentration profiles to derive a theoretical criterion for the occurrence of this morphology. In general, the internal oxidation can occur when the depleted reactive solute exhibits very slow diffusion, while the solubility and diffusivity of oxygen in the alloy are relatively high. Smeltzer and Whittle[3] have recently extended the analysis to include cross-effects in the diffusion of the components.

Table I. Composition of Ni–Cr–W Alloys[a]

Alloy designation	Wt.% Cr	At.% Cr	Wt.% W	At.% Cr
Ni–30Cr	26.2	28.6	0	0
Ni–Cr–1.6W	18.7	21.3	5.0	1.60
Ni–Cr–3W	20.0	23.4	9.1	3.0
Ni–Cr–6W	18.7	23.3	17.8	6.3
Ni–Cr–10W (two-phase)	16.2	22.0	27.3	10.4

[a]Metal impurities <0.1 wt.%.

In this research, the Wagner mechanism for oxidation of Cu–Pt and Cu–Pd alloys is generalized and examined for ternary alloys where the rejected solute is not strictly a noble metal, but rather one which depends upon the protective scale for the prevention of a more accelerated oxidation of the underlying composition. For example, in Ni–Cr–W alloys containing sufficient Cr for the formation of a Cr_2O_3 external scale, the simultaneous precipitation of Cr_2O_3 by internal oxidation would deplete the alloy of that component required to maintain the growth of the protective scale. This circumstance could lead to such an increase in oxygen activity at the alloy–scale interface that the oxidation of the second-most-reactive component (W in Ni–Cr–W alloys) could lead to fracture of the protective scale and breakaway oxidation.

In this study of the high-temperature oxidation of Ni–Cr–W alloys, thermogravimetric, structural, microstructural, and compositional analyses were made and are reported.

EXPERIMENTAL MATERIALS AND PROCEDURES

The experimental Ni–Cr, Ni–Cr–W alloys listed in Table I were prepared from high-purity (99.95 wt.%) tungsten and electrolytic (99.9 wt.%) nickel, and chromium. The Ni–Cr–10W alloy was two-phase, composed of sigma particles in the alloy fcc matrix.

The alloys were first melted in a vacuum induction furnace, and then arc melted in argon. The alloys were hot rolled at 1370°C to a thickness of ~1.6 mm. After the final roll the alloys were annealed for 15 min at 1350°C and air cooled to room temperature. Finally they were annealed at 1100°C in argon for 5.5 hr and subsequently water quenched. Samples cut from these annealed alloy sheets were ground and polished. Final polishing was done with 1 μ diamond paste. The dimensions of the oxidation samples were $10 \times 10 \times 1.2$ mm.*

*Some of the alloy fabrication was done at Battelle Memorial Institute, Columbus, Ohio.

The oxidation rates were measured with a Cahn R-100 recording balance mounted above a vertical furnace. All oxidations were performed in air and the samples were lowered directly into the preheated furnace and suspended on the balance at the start of an experimental run.

The samples were mounted for metallographic examination between two microscope slides to preserve edges. The reaction products were analyzed using X-ray diffraction, metallographic techniques, an electron microprobe, and a scanning electron microscope in the back-scattered electron mode and secondary electron mode. An empirical correction method[4] was used for the quantitative analysis of the microprobe data. The Ni–Cr–3W alloy and the pure elements were used as standards. Only background corrections were made for the analysis of oxides.

RESULTS

Thermogravimetric Studies

Measurements of the oxidation rate of the experimental alloys in Table I were performed in air at 1 atm total pressure in the temperature interval 1000–1250°C. The kinetic results are shown in Figs. 1–4.

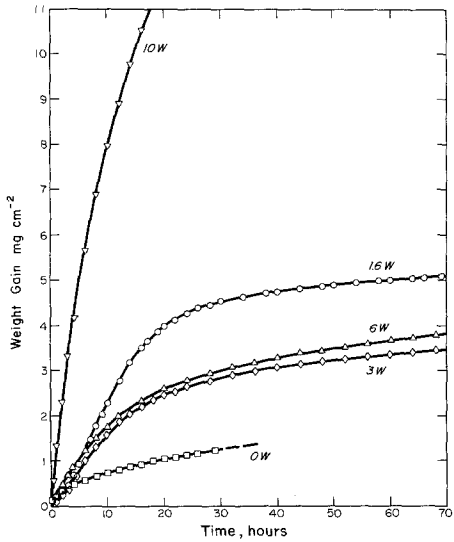

Fig. 1. Weight gain for Ni–30Cr, Ni–Cr–1.6W, Ni–Cr–3W, Ni–Cr–6W, and Ni–Cr–10W alloys oxidized in air at 1000°C.

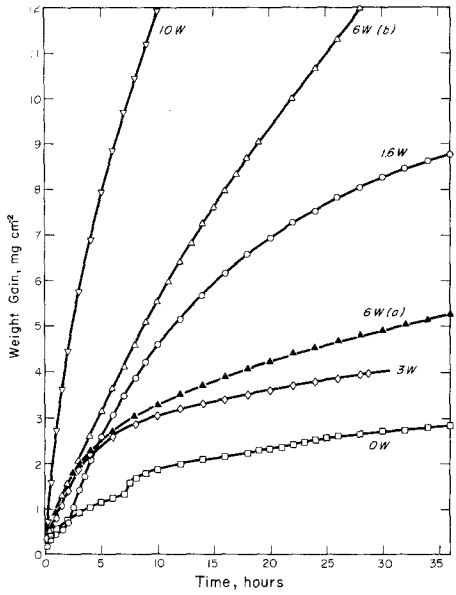

Fig. 2. Weight gain for Ni–Cr–W alloys oxidized in air at 1100°C.

Figure 1 shows the weight gain per unit area (mg/cm^2) for oxidation of the alloys in air at 1000°C. The Ni–Cr–10W oxidizes rapidly, 8 mg/cm^2 in 10 hr. The Ni–Cr–W alloys containing less W show rapid oxidation rates initially, which drop after some time. The Ni–30Cr alloy was oxidized for

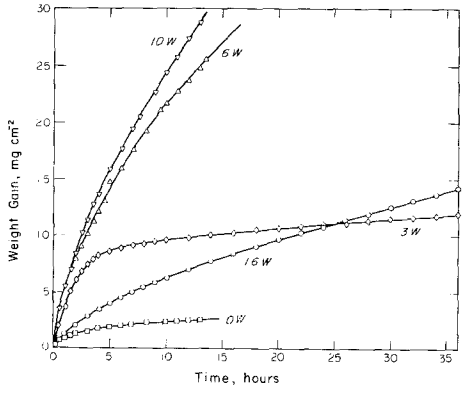

Fig. 3. Weight gain for Ni–Cr–W alloys oxidized in air at 1200°C.

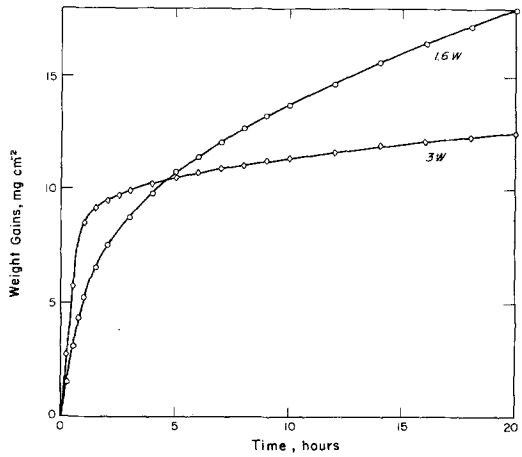

Fig. 4. Weight gain for Ni–Cr–1.6W and Ni–Cr–3W alloys oxidized in air at 1250°C.

comparison. The alloys with 1.6, 3, and 6 W oxidize with approximately the same rate as the Ni–30Cr alloy after long (~40 hr) exposure.

Figure 2 shows weight gains for oxidation at 1100°C. The oxidation rate of the Ni–Cr–6W alloy varied considerably from sample to sample as can be seen from curves for duplicate experiments labeled 6W(a) and 6W(b). The sample Ni–Cr–6W(a) exhibited kinetics somewhat similar to those of the Ni–Cr–3W alloy while the Ni–Cr–6W(b) sample oxidized much faster. Later, this difference in behavior is shown to correspond to differing scale morphologies.

Figure 3 shows oxidation kinetics at 1200°C. Four different types of oxidation behavior seem to occur. Both the Ni–Cr–6W and Ni–Cr–10W alloys oxidized at about the same high rate and by similar mechanisms. The Ni–Cr–3W alloy has about the same initial oxidation rate as the 6W and 10W alloys for the first 2 hr, but then the rate drops and eventually approximates the oxidation rate of the Ni–30Cr alloy. The initial kinetics for the Ni–Cr–1.6W alloy are comparable with those for the Ni–30Cr alloy, but the oxidation continues according to a linear rate law (approximately) and therefore does not drop as quickly as the approximate parabolic rate observed for the Ni–30Cr alloy.

The oxidation kinetics of Ni–Cr–1.6W and Ni–Cr–3W alloys were also measured at 1250°C. The results, presented in Fig. 4, are similar to the results obtained at 1200°C. The Ni–Cr–3W alloy has initially a higher oxidation rate, but this rate drops drastically between 1 and 5 hr of exposure. The Ni–Cr–1.6W alloy starts out with a lower oxidation rate than the

Ni–Cr–3W alloy, but after 5 hr of oxidation the weight gains of the two alloys are comparable.

Analysis of Oxidized Samples

a. The oxides positively identified by X-ray diffraction on specimens oxidized 30 hr at 1200°C are presented in Table II.

At the external surfaces of the oxide scales formed on the alloys, NiO was found. Closer to the scale–metal interface, $NiWO_4$ plus $NiCr_2O_4$ and/or Cr_2O_4 were found. Similar results were obtained at other temperatures. For 1000°C oxidation, the Ni–Cr–6W alloy definitely showed Cr_2O_3 formation beneath a NiO layer with some $NiWO_4$ present.

b. Metallographic, microprobe, and scanning electron microscope examinations were made on the oxidized specimens. Figure 5a is a back-scattered electron micrograph of the scale cross section on the Ni–Cr–10W alloy oxidized at 1000°C for 30 hr. The outer columnar oxide is NiO. The underlying oxide layer is a stratified mixture of oxides. Because of its high atomic weight, the tungsten-rich oxide shows up as bright areas. The scale–alloy interface is shown in Fig. 5b. The sample was relief (excessively) polished to show the second-phase W precipitates in the alloy matrix. The interface is very ragged and the internal oxides are rich in chromium, certainly being Cr_2O_3. The fast oxidation rate arises because of the absence of a continuous Cr_2O_3 layer at the metal–scale interface. Chromium oxidizes internally and the other, more noble, elements (Ni, W) oxidize as the interface progresses. The inner scale is very porous and brittle, and the stratification of W suggests a repeated fracturing of an ineffective protective scale.

Relative to the transport processes responsible for scale growth, the presence of $NiWO_4$ particles throughout the scale indicates that some scale is formed at the metal–scale interface by the ingress of oxygen-containing molecules according to the frequently discussed "dissociation" mechanism.[5]

Table II. Oxides Identified by X-Ray Diffraction on Specimens Oxidized Approximately 30 hr at 1200°C in Air

Alloy designation	Oxides positively identified (outer/inner)
Ni–30Cr	Cr_2O_3
Ni–Cr–1.6W	[a]
Ni–Cr–3W	NiO/Cr_2O_3, $NiWO_4$, $NiCr_2O_4$
Ni–Cr–6W	$NiO/NiCr_2O_4$, $NiWO_4$
Ni–Cr–10W	$NiO/NiWO_4$, $NiCr_2O_4$

[a]Not analyzed.

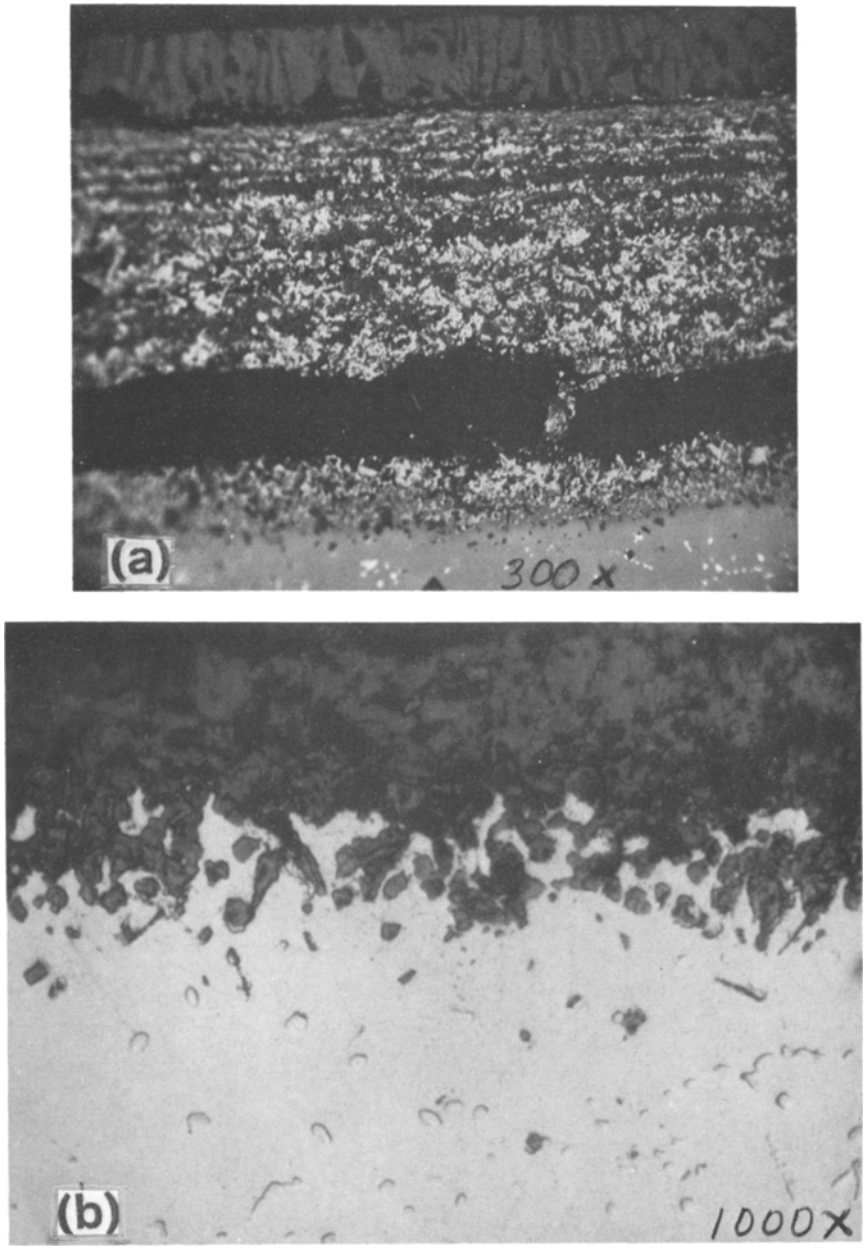

Fig. 5. (a) Scale formed on a Ni–Cr–10W alloy oxidized at 1100°C for 30 hr; back-scattered electron photomicrograph, ×300; (b) scale formed on a Ni–Cr–10W alloy oxidized at 1100°C for 30 hr; optical micrograph of the oxide–alloy interface, ×1000.

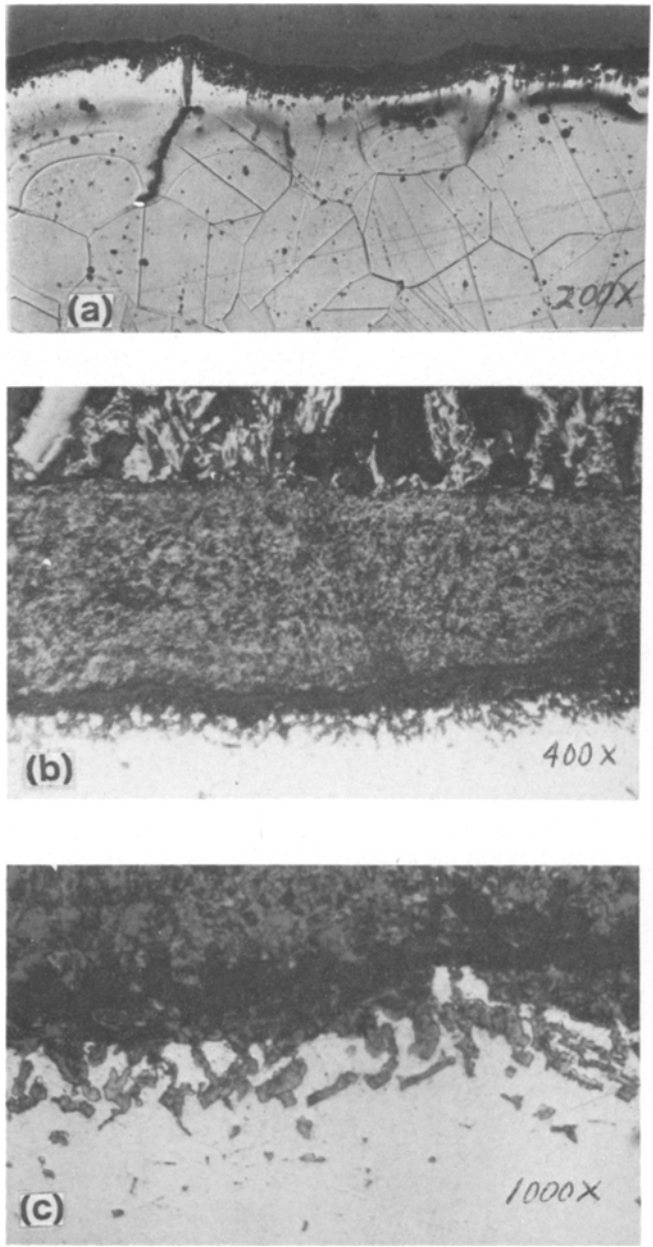

Fig. 6. Scale formed on Ni–Cr–6W alloys oxidized in air at 1100°C for 30 hr (oxidation curve marked 6W(b) in Fig. 2): (a) etched to reveal grain boundaries in the alloy, ×200; (b) entire oxide, ×400; (c) oxide–alloy interface, ×1000. All parts reduced 25% for reproduction.

This oxidation mode is facilitated by the inevitable presence in the initial alloy of some carbon or hydrogen which provides CO_2 or H_2O molecules to assist oxygen transport through a porous scale for oxide formation at the alloy–scale interface.

Figures 6a, 6b, and 6c are photomicrographs of the scale–alloy interface for the Ni–Cr–6W alloy oxidized 30 hr at 1100°C, corresponding to the curve marked 6W(b) in Fig. 2. The micrographs of Figs. 6b and 6c resemble those of Figs. 5a and 5b for the Ni–Cr–10W alloy and suggest a similar nonprotective mechanism. The internal Cr_2O_3 particles for the 6W alloy are larger and some protective oxide has formed at two grain boundaries in Fig. 6a, as indicated by a reduced metal recession in that region. The morphologies of the Cr_2O_3 grain-boundary precipitates resemble closely those previously reported in comprehensive studies of the oxidation of binary Ni–Cr alloys.[6,7] However, the grain boundary Cr_2O_3 films have not interconnected to achieve a transition to continuous, protective Cr_2O_3 scales on the high-W alloys.

Figures 7a and 7b are photomicrographs of the Ni–Cr–6W alloy oxidized at 1000°C which show that the grain boundaries are lined with oxide. The oxidation kinetics of this sample were given in Fig. 1. Figure 7b shows some continuous chromium oxide formation along grain boundaries. Figure 7c is a back-scattered electron micrograph of an area adjacent to that depicted in Fig. 7b; the bright areas are rich in tungsten. Figure 8 is a microprobe trace across the section shown in Fig. 7c. The outer 20–25 μ of the oxide layer is almost pure NiO. A small amount (~2%) of Cr has dissolved in the NiO at its inner interface. This magnitude for the solubility for Cr in NiO agrees with the microprobe results of Wood and Hodgkiess[8] and the electrical conductivity studies of Meier and Rapp.[9]

Immediately beneath the outer NiO scale is a layer seen best as the W-free, dark band in Fig. 7c, which is interpreted to be $NiCr_2O_4$. The microprobe trace of Fig. 8 shows that this thin layer contains both Ni and Cr but essentially no tungsten. Unfortunately, the microprobe could not accurately define the Ni:Cr ratio in this thin layer about 2.5 μ thick. The white $NiWO_4$ particles of Fig. 7c are obviously excluded (rejected) from this thin $NiCr_2O_4$ layer.

Further, from Figs. 7c and 8, although considerable Cr_2O_3 is present in the scale, a continuous layer of Cr_2O_3 at the metal–scale interface is definitely not present. The remarkable conclusion derived from these observations is that the intermediate $NiCr_2O_4$ layer must be the protective layer responsible for the slow long-term kinetics of the 6W alloy in Fig. 1. The only alternative conclusion would require the aggregate duplex scale of Cr_2O_3, $NiWO_4$, and $NiCr_2O_4$, and probably NiO to limit the kinetics—an unlikely choice. While $NiCr_2O_4$ and other spinels are known to exhibit low

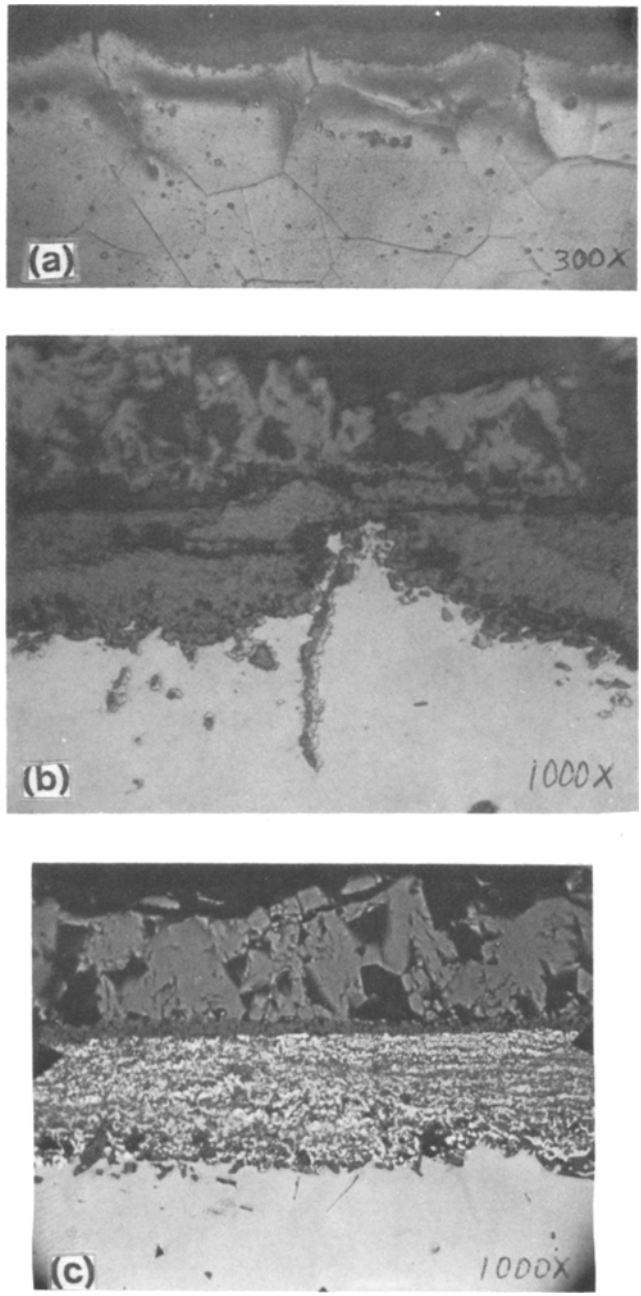

Fig. 7. Scale formed on Ni–Cr–6W alloy oxidized at 1000°C for 80 hr: (a) etched to reveal grain boundaries, ×300; (b) oxides along grain boundary; (c) back-scattered electron micrograph of area adjacent to (b). All parts reduced 25% for reproduction.

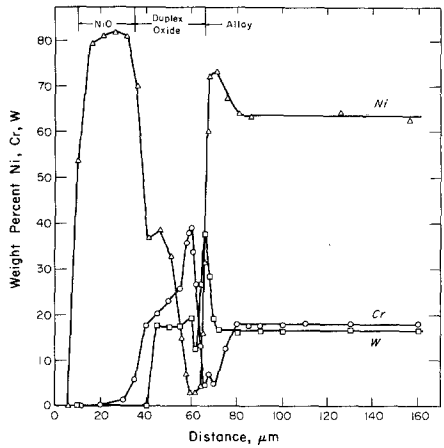

Fig. 8. Microprobe concentration profile of Ni–Cr–6W alloy oxidized at 1000°C for 80 hr across area of Fig. 7c.

ionic diffusivities,[10] only seldom are the two cation species found in the proper proportion at a given location in a scale so that a compact protective spinel layer is formed.

In Fig. 8 the microprobe trace shows a substantial W enrichment in the alloy beneath the oxide, as well as Cr depletion from ~18 wt.% down to ~5 wt.%. The depth of the Cr depletion is greater than the depth of W enrichment, which partially reflects the difference in their diffusion coefficients. However, the occurrence of the internal oxidation of Cr provides further removal of Cr from solid solution. The oxidation rate of this sample is very low, comparable with the oxidation rates of Ni–Cr–3W and Ni–30Cr for the same experimental conditions. For these two alloys, the slow kinetics correlate with the microprobe detection of considerable Cr_2O_3 adjacent to the metal. However, for the Ni–Cr–6W alloy a compact internal film of protective Cr_2O_3 is not evident, either in the photomicrographs or from the microprobe trace.

Figures 9a and 9b are photomicrographs and microprobe traces for differing scales formed on a Ni–Cr–3W specimen oxidized at 1200°C for 40 hr. In Fig. 9a, a dense and strongly adherent Cr_2O_3 layer is seen. Most of the outer NiO layer has spalled away. Figure 9b depicts an area with thicker oxide formation.

For the uniformly protective oxide morphology of Fig. 9a, the oxide scale does not contain any tungsten, which is completely partitioned to the metal (rejected) at the oxide–metal interface. There is about 17.5 wt.% W at

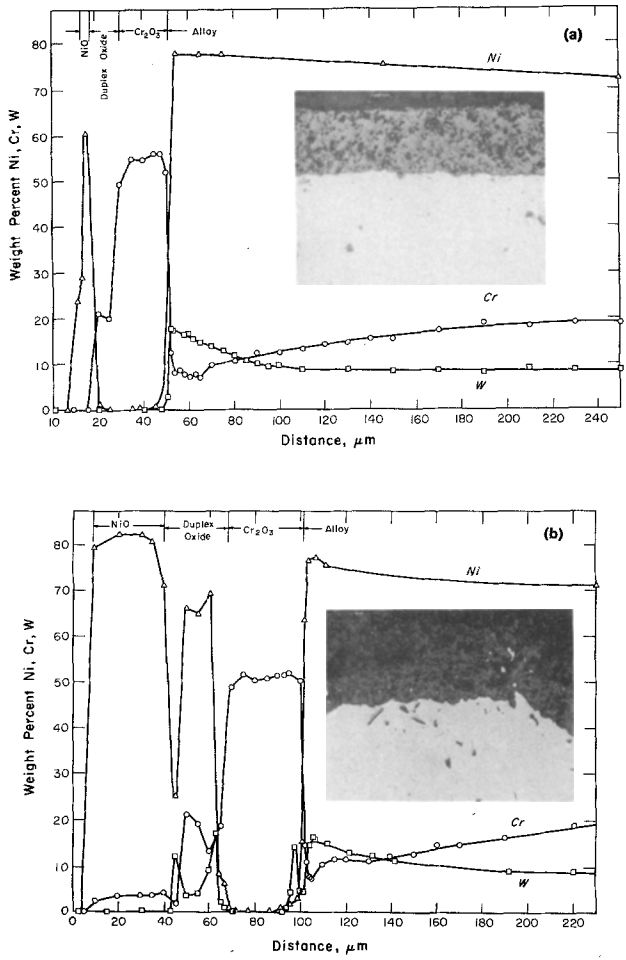

Fig. 9. (a) Micrograph (×1000) and microprobe analysis of scale formed on Ni–Cr–3W alloy oxidized 40 hr at 1200°C. (b) Same as (a), for a different scale. All parts reduced 70% for reproduction.

the alloy–scale interface. The tungsten gradient extends for about 50 μ into the alloy, while the chromium depletion gradient extends about 150 μ into the metal. The Cr content in the alloy just beneath the oxide is about 12.5 wt.%, compared with the 20.0 wt.% of the initial alloy.

Figure 9b presents a microprobe trace across an oxide scale layer with a thicker, irregular morphology. The protective Cr_2O_3 layer has not formed as fast as for the area depicted in Fig. 9a. The outer oxide in Fig. 9b is NiO, which is about 30 μ thick and contains ~3.5 wt.% Cr. Beneath the NiO

layer is a stratified scale containing W, Ni, and Cr, with a thick Cr_2O_3 layer beneath these oxides adjacent to the metal. The W rejection is not as great as for the dense uniform oxide scale. The interface between the oxide and the metal is not straight, which might account for the "irregularities" in the profiles inside the metal. The electron beam might also have encountered one or several small internal oxide particles. Metal particles are also incorporated (enveloped) into the oxide, as seen in Fig. 9b.

Figure 10 shows optical and back-scattered scanning electron microscope (SEM) micrographs of the oxide scale formed on a Ni–Cr–3W sample oxidized at 1250°C for 122 hr. The corresponding kinetic curve of Fig. 4 indicates a rapid initial oxidation rate followed by protective behavior. A columnar NiO scale layer is found at the external surface. A thick Cr_2O_3 scale is also seen between the alloy and the NiO. In the region between the NiO and the Cr_2O_3 there are phases which are probably $NiWO_4$ and $NiCr_2O_4$. Some oxidized tungsten is also observed in the Cr_2O_3 layer.

Figures 11a and 11b are SEM (secondary electron) micrographs of the edge and middle of the outer surface of the external NiO scale on the same 3W alloy oxidized at 1250°C for 122 hr. Solid crystallites appear on the surface, rounded off because of evaporation. No evidence of a liquid phase was observed on the surface. This outer NiO scale layer was probably effective in reducing the CrO_3 evaporation from the alloy. The protective kinetics for this alloy at the very high temperature of 1250°C indicate that the presence of W in the alloy does not necessarily lead to the breakaway, catastrophic oxidation resulting from the formation of WO_3 liquid or vapor.

Figure 12 shows a photomicrograph and a microprobe concentration profile for scale formed on a Ni–Cr–1.6W sample oxidized at 1200°C for 45 hr. The corresponding kinetic curve is shown in Fig. 3. The tungsten is completely rejected to the alloy at the alloy–oxide interface. However, the maximum tungsten concentration observed in the underlying alloy is only ~8.5 wt.%. A dense, protective Cr_2O_3 layer with traces of external NiO makes up the scale structure.

Figure 13 shows micrographs of other (nonprotected) areas on the same Ni–Cr–1.6W sample as in Fig. 12. In the areas shown in Fig. 13, the protective external Cr_2O_3 layer was either damaged, had voids in it, or could not form. In Fig. 13a, the locally rapid oxidation rate of the grain below the alloy–scale interface may be on the verge of healing if the extension of the Cr_2O_3 grain boundary film is able to isolate the outer grain before extensive internal oxidation can deplete chromium from the underlying grain. In Fig. 13b, the external protective Cr_2O_3 layer seems to have spalled off at temperature. Internal Cr_2O_3 oxides have formed and a grain boundary in the alloy, which is necessary to initiate a "healing" internal Cr_2O_3 film, is locally unavailable. The existence of locally unprotected areas such as shown

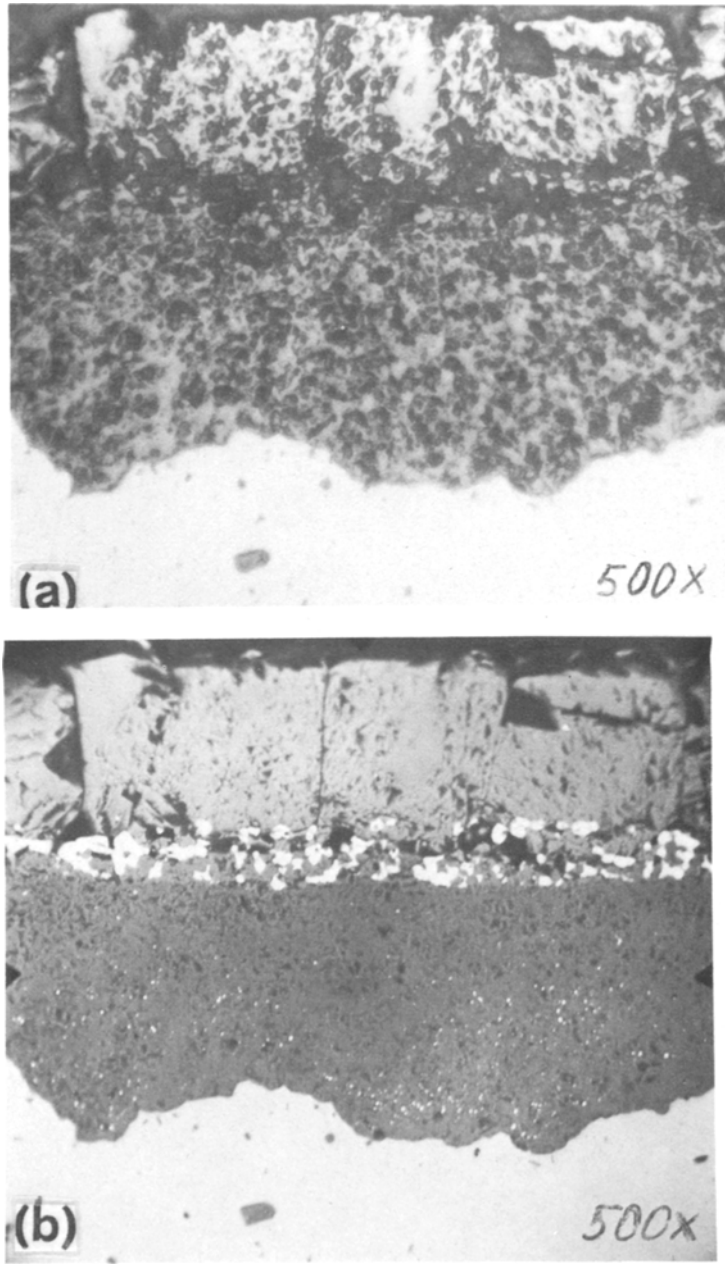

Fig. 10. Optical micrograph (×500) and back-scattered SEM micrograph (×500) of scale formed on Ni–Cr–3W alloy oxidized at 1250°C for 122 hr.

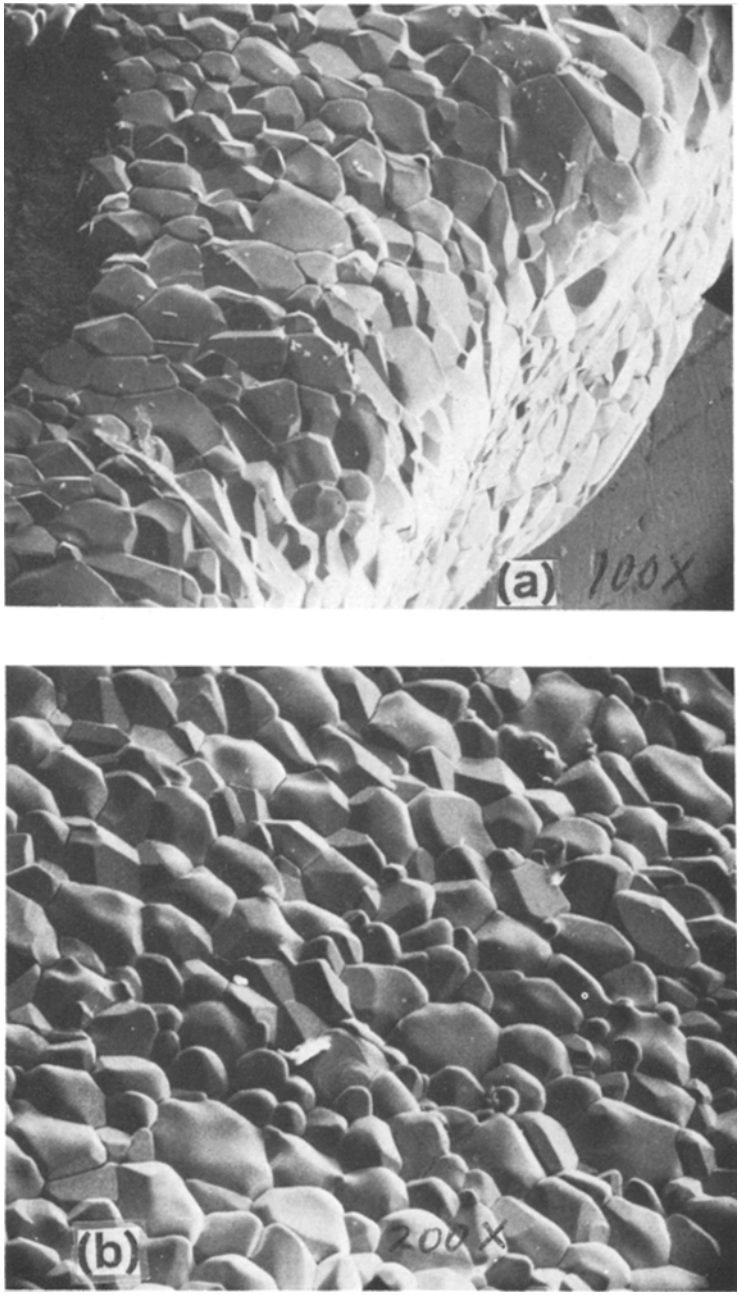

Fig. 11. Scanning electron micrograph (secondary electrons) of NiO surface oxide on a Ni–Cr–3W sample oxidized 122 hr at 1250°C: (a) edge; ×100; (b) fault surface, ×200.

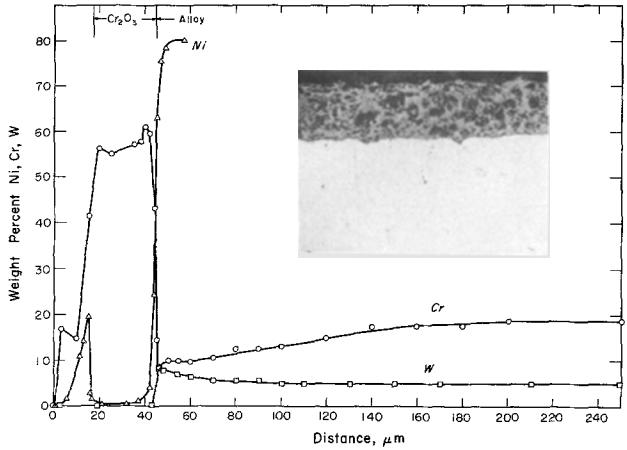

Fig. 12. Microprobe concentration profile for scale formed on Ni–Cr–1.6W alloy oxidized at 1200°C for 45 hr; optical micrograph at ×1000, reduced 70% for reproduction.

in Fig. 13 causes the long-term higher oxidation kinetics for the Ni–Cr–1.6W specimen in Fig. 3 compared with those for the Ni–Cr–3W specimen.

The previously presented micrographs show reaction products on samples oxidized 30 hr or longer. Substantial differences exist in the oxidation behavior of Ni–Cr–1.6W, Ni–Cr–3W, and Ni–Cr–6W alloys at 1200°C, especially after 4 hr of oxidation when the Ni–Cr–3W alloy exhibits a drastically reduced rate. One sample of each of these alloys was oxidized at 1200°C for 4 hr. The resulting alloy–scale interfaces and kinetics are shown in Fig. 14. The Ni–Cr–6W alloy shows large internal Cr_2O_3 oxides and a very ragged interface with no continuous, protective Cr_2O_3 layer. A second metallic phase, probably sigma phase, is seen to coat the internal Cr_2O_3 precipitates.

The Ni–Cr–3W is in the process of forming a continuous Cr_2O_3 layer, as can be seen in Fig. 15, which is a microprobe scan across the entire oxide formed at 1200°C for 4 hr. A protective Cr_2O_3 layer about 5–10 μ thick exists in contact with the alloy. Again, a second phase appears in the alloy adjacent to Cr_2O_3. Protective Cr_2O_3 has formed on large proportions of the Ni–Cr–1.6W surface, but several areas still show extensive internal oxidation.

DISCUSSION OF EXPERIMENTAL RESULTS

The interpretation of the oxidation behavior of Ni–Cr–W alloys will be divided into a discussion of (a) nonprotective behavior for the highest W

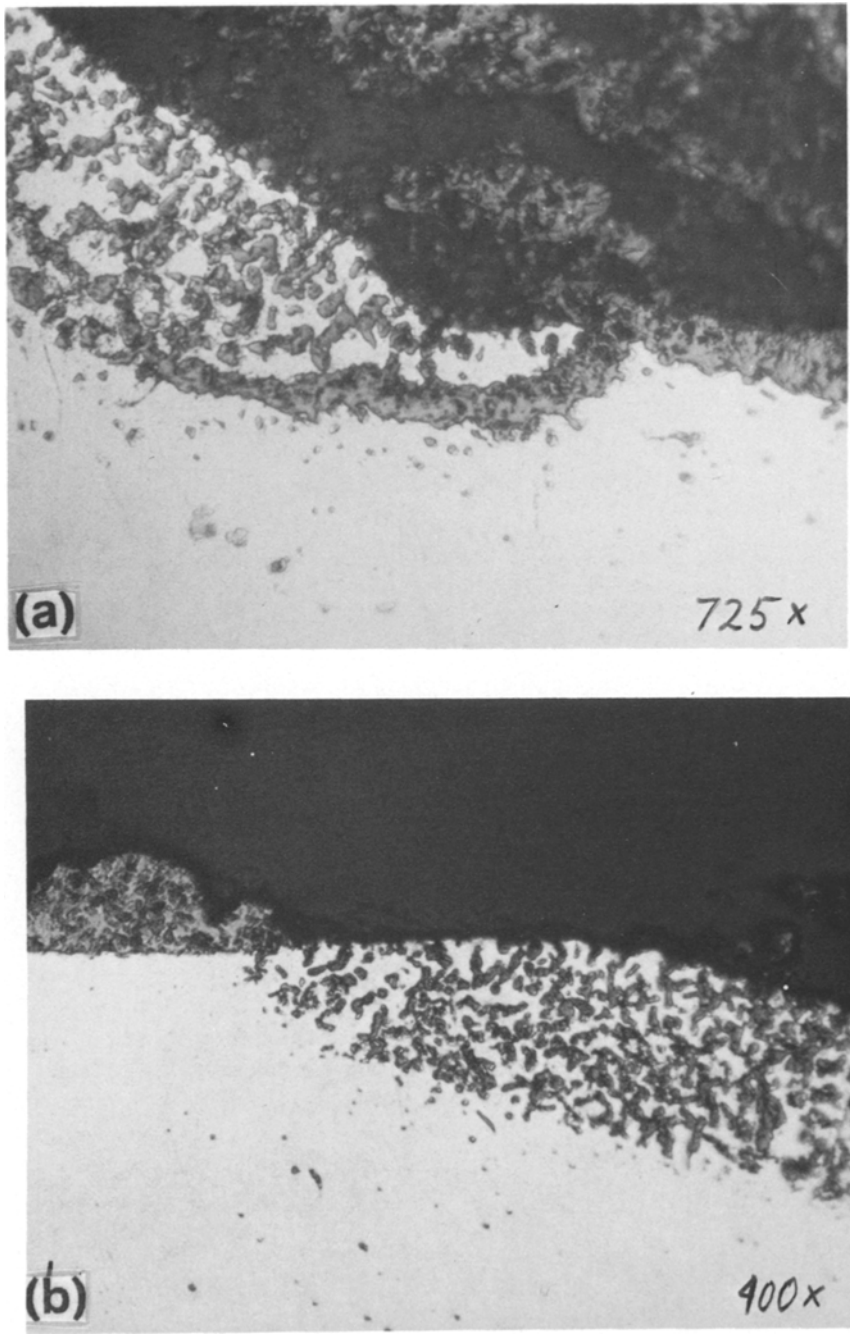

Fig. 13. Internal oxides formed in Ni–Cr–1.6W alloy oxidized 45 hr at 1200°C: (a) ×725; (b) ×400.

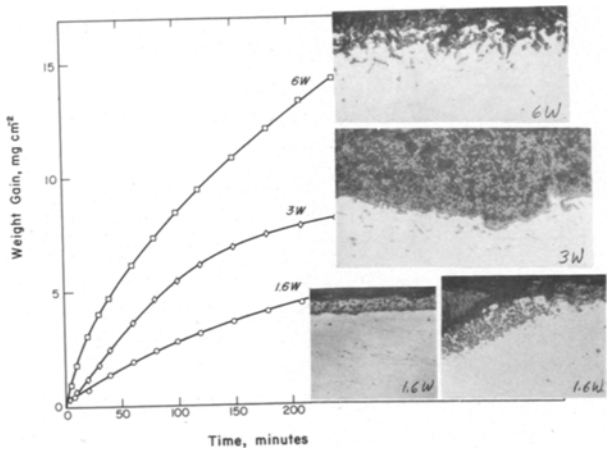

Fig. 14. Microstructures and weight gains for Ni–Cr–1.6W, Ni–Cr–3W, and Ni–Cr–6W alloys oxidized 4 hr at 1200°C × 725; reduced 70% for reproduction.

alloy (10W) and mixed behavior of the 6W alloy; (b) protective oxidation for the intermediate (3W) composition; and (c) irregular behavior for the lowest W alloy (1.6W). From Figs. 1–3, the 6W alloy is protective at 1000°C, nonprotective at 1200°C, and at 1100°C its behavior is irregular.

As shown in Fig. 3, Ni–Cr–6W and Ni–Cr–10W alloys oxidize at the same high initial rate at 1200°C. From Figs. 5 and 6, in an unprotected alloy, NiO is formed as an external scale above a duplex, stratified layer consisting

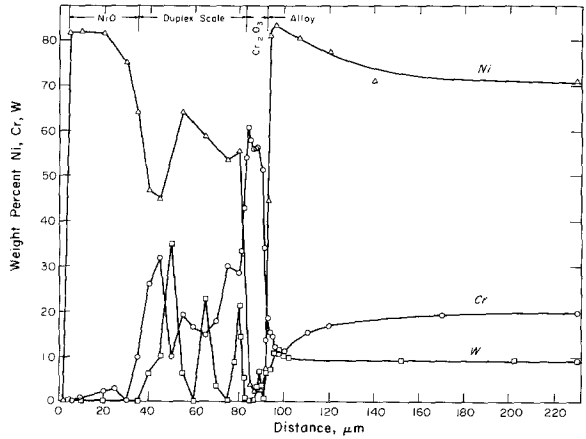

Fig. 15. Microprobe concentration profile of oxide formed on a Ni–Cr–3W alloy oxidized 4 hr at 1200°C in air.

of $NiCr_2O_4$, $NiWO_4$, and some NiO and Cr_2O_3. Large internal Cr_2O_3 particles are precipitated in the alloy and the noble solutes W and Ni are partitioned in high concentration around and in advance of the internal precipitates. Grain-boundary Cr_2O_3 films are not in evidence. The stratification of the W and Cr components in the scale of Fig. 5a suggests that at numerous times in the earlier oxidation stages, protective films were formed at the alloy–scale interface upon the interconnection of Cr_2O_3 particles; obviously this protection was not lasting, because of renewed internal precipitation of Cr_2O_3 in the alloy beneath a zone of Cr depletion and W enrichment. Along the alloy grain boundaries a similar effect of excessive rejected W solute retards the arrival of chromium for the formation of "healing" grain-boundary Cr_2O_3 films. Finally, at later times, the repeated formation and failure of localized protective films by renewed internal Cr_2O_3 precipitation becomes so randomized along the alloy–scale interface that even temporary formation of Cr_2O_3 films is not possible. For the rapidly oxidizing 6W alloy of Fig. 6 at 1100°C, some tendency for the formation of Cr_2O_3 grain-boundary films is shown, but the large grain size prevents a realization of reduced kinetics by this healing mechanism. Only at 1000°C, where an intermediate continuous protective layer of $NiCr_2O_4$ spinel forms, is the oxidation rate of the 6W alloy reduced.

Relative to the role of W in high-W alloys on the oxidation kinetics and scale morphology, the effect is consistent with that previously suggested by Wagner[2] to explain the internal precipitation of Cu_2O particles beneath a Cu_2O scale on Cu–Pt and Cu–Pd alloys. The activity of oxygen at the Ni–Cr–W alloy–scale interface exceeds that deeper in the alloy because the reactive Cr component is depleted at the interface while the noble components, W and Ni, are locally concentrated. This differential oxygen activity is sufficient to accomplish the internal oxidation of Cr to Cr_2O_3 if Wagner's kinetic criterion is satisfied. For high-W, Ni–Cr–W alloys this criterion was obviously met, although data are not available for quantitative evaluation.

The gravimetric parabolic oxidation rate constant k_g in the expression $(\Delta W/A)^2 = k_g t$ is given by

$$k_g = 0.13 \exp(-45{,}800/RT) \text{g}^2/\text{cm}^4\text{-sec}$$

for the formation of duplex scale on the Ni–Cr–10W alloy. This expression represents a rate which is about one order of magnitude faster than the oxidation of pure Ni[11] at 1000–1200°C. Because the oxygen activity throughout the scale is oxidizing to both the W and Cr component, some doping of W and Cr into the matrix NiO phase of the scale could contribute to the rapid parabolic scaling rate. Also, the formation of Cr_2O_3 internal

precipitates serves to initiate and maintain a porous inner scale layer in support of the dissociative oxidation mechanism.

For the Ni–Cr–3W alloy at all temperatures, and for the 1.6W and 6W alloys at 1000°C, a slow steady-state oxidation rate, comparable with that of a Ni–30Cr alloy, was observed. However, the W-containing alloys always exhibited faster initial (transient) rates during which NiO was formed as an outer scale layer. Generally, the eventual formation of a protective Cr_2O_3 film at the metal–scale interface provided the slower steady-state kinetics. As an unusual instance seen in Figs. 7c and 8, the protective layer on the 6W alloy at 1000°C was apparently a $NiCr_2O_4$ spinel layer which formed between the inner duplex scale and an outer NiO scale layer.

The success of the 3W alloy in resisting oxidation over the entire range from 1000 to 1250°C at first appears somewhat puzzling, considering that a lower W content of 1.6W was not so effective. A review of Figs. 9a, 9b, 10, and 14, however, shows that the oxidation-resistant 3W alloy exhibited much less internal oxidation than the 6W or 10W alloys. Likewise, the local failure of the 1.6W alloys (Figs. 13 and 14) corresponded to the occurrence of profuse internal oxidation. While the growth of healing grain-boundary Cr_2O_3 films is known to form protective scales, the large grain size of these alloys probably minimized the importance of this contribution. While scale adherence was not specifically tested by subjecting the alloys to temperature cycling, the roughened alloy–scale interfaces of Figs. 9a, 9b, 10, and 14 would suggest that the addition of 3W would assist scale adherence. A roughening of the interface is a general expectation as diffusion in the alloy contributes to the rate control.[12]

Parabolic rate constants were calculated from the kinetic data for conditions where it was found metallographically that the sample was completely covered with a protective Cr_2O_3 layer. This could be done only for the Ni–30Cr and Ni–Cr–3W alloys. The results are shown in Fig. 16, where k_g, the parabolic (gravimetric) rate constant in $g^2/cm^4 \cdot sec$ (from the equation $(\Delta W/A)^2 = k_g t$), is plotted against $10^4/T$. Data from a similar investigation on Co–Cr–W alloy are included.[13] An experimental k_g value for pure Cr oxidized at 0.1 atm O_2 at 1000°C is plotted. The line labeled (a) is calculated from Wagner's parabolic oxidation rate theory with the equation

$$k_p = \frac{C_{eq}}{2} \int_{P_{O_2}(Cr/Cr_2O_3)}^{P_{O_2}(Cr_2O_3/O_2)} \left[\frac{z_c}{z_a} D_c^* + D_a^* \right] d \ln P_{O_2}$$

where C_{eq} is the equivalents/cm^3 for Cr_2O_3, z_c and z_a are the valences of the cations and anions in the scale, and D_c^* and D_a^* are their self-diffusion coefficients. The relation between k_g and k_p is:

$$k_g = (2\rho_{ox}^2 / C_{eq}) k_p$$

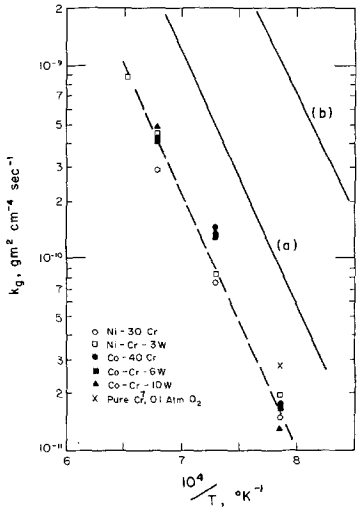

Fig. 16. The parabolic rate constants, k_g, for protective oxidation for Ni–30Cr and Ni–Cr–3W alloys; k_g values from a similar study on Co–Cr–W alloys are included. Line (a) is calculated from Wagner's parabolic rate theory using $D_{Cr}^{Cr_2O_3} = 0.167 P_{O_2}^{3/16} \exp(-61{,}100/RT)$ and (b) using $D_{Cr}^{Cr_2O_3} = 0.167 \exp(-61{,}100/RT)$.

where ρ_{ox} is grams oxygen per cm^3 in the oxide. Anion diffusion in Cr_2O_3 is known to be much less than cation diffusion, and the data used for Cr diffusion are

$$D_{Cr}^{Cr_2O_3} = 0.167 P_{O_2}^{3/16} \exp(-61{,}100/RT)$$

In this equation the pressure dependence of $D_{Cr}^{Cr_2O_3}$ demonstrated by Walters and Grace[14] has been added to the tracer diffusion expression of Hagel and Seybolt.[15]

The line (b) of Fig. 16 plots k_g calculated from the expression $D_{Cr}^{Cr_2O_3} = 0.167 \exp(-61{,}100/RT)$, i.e., as reported by Hagel and Seybolt without any P_{O_2} dependence.

No significant differences exist in the oxidation rates of Co–Cr, Co–Cr–W, Ni–Cr, and Ni–Cr–W alloys when Cr_2O_3 is the protective oxide formed on these alloys. A differential doping effect by Co, Ni, or W in the growth of Cr_2O_3 is not important for these alloys. The dashed line through the experimental rate constants in Fig. 16 has an activation energy of 66 kcal/mole, in agreement with the activation energy of Cr diffusion in sintered polycrystalline Cr_2O_3 as found by Hagel and Seybolt. The comparison of these experimental data with the alternative calculated lines (a) and (b) suggests that the inclusion of the $P_{O_2}^{3/16}$ dependence in the diffusivity, $D_{Cr}^{Cr_2O_3}$, provides better agreement, but a factor of about 5 still separates the computed and the experimental values, with the experimental values being lower. One factor contributing to a slower Cr_2O_3 growth rate relative to that calculated is the fact that for the alloys, a layer of NiO or CoO covers the Cr_2O_3 interface, so that the oxygen activity at the outer boundary

of the Cr_2O_3 scale must be considerably less than the 0.21 atm oxygen used in calculating k_g.

Caplan and Sproule[16] have compiled the rate constants for the oxidation of chromium. The data for the growth of polycrystalline Cr_2O_3 scales generally scatter within one order of magnitude of the data in Fig. 16. However, the thickening of individual (single-crystal) grains of Cr_2O_3 occurs at a rate which is slower by a factor of 30 to 90. These single crystals thickened according to an activation energy of 58 kcal/mole. Recent tracer diffusion data[17] for Cr in Cr_2O_3 single crystals correspond to this much slower rate rather than that reported by Hagel and Seybolt[15] for sintered powder specimens. In particular, in the light of recent comprehensive studies on the growth of polycrystalline NiO, Cu_2O, Al_2O_3, and Cr_2O_3 scales, there is general agreement that growth of these scales at intermediate temperatures is limited by short-circuit, grain-boundary diffusion, perhaps with a contribution by oxygen anions. The current experiments with ternary alloys were not designed to contribute fundamental information relative to the growth mechanism of Cr_2O_3 scales. However, the agreement in activation energies for Cr tracer diffusion in Cr_2O_3 or growth of single-crystal Cr_2O_3 and the growth of polycrystalline Cr_2O_3 scales by short-circuit diffusion is noteworthy.

SUMMARY AND CONCLUSIONS

The sequence of decreasing oxidation rates for the 10W, 6W, and 3W alloys is readily explainable in terms of the Wagner-type model for Cu–Pd alloys.[2] Tungsten rejection to the metal phase reduces the Cr activity at the metal–scale interface, permitting internal oxidation of Cr. Rejection of W around these internal oxides further reduces the local Cr activity and tends to promulgate internal oxidation in preference to formation of a protective continuous layer. The effect is greater the greater the W content, accounting for the observed trend in oxidation rates. A secondary effect to that of Cr depletion is the reduction of Cr diffusivity with increased W, which would accentuate the depletion as well as the trend to internal oxidation with increased W content. The negative interaction coefficient between Cr and W implied by the intermetallic compound formation in the Ni–Cr–W system suggests such a decrease in diffusivity and for the parallel case of Ni and W, W has been found to reduce the diffusivity of Ni.[18]

The lower W in the 1.6W alloy should cause less impedance to Cr arrival at the scale–metal interface and less internal oxidation by the above model. However, for these alloys, as shown in Fig. 14, a Cr_2O_3 scale forms at such an early stage that a much thinner NiO outer layer is present. The thinner layer of outer NiO and presumably intermediate $NiCr_2O_4$ may

permit an increased availability of oxygen to the initial protective Cr_2O_3 and thereby somehow accentuate local instances of spalling, and again internal oxidation of Cr_2O_3 in preference to continued protective film growth. Hence, the best W concentration for maximizing isothermal oxidation resistance in the range 1000–1250°C for Ni–20Cr–W alloys is the 3W alloy of those studied, and the optimum concentration lies somewhere in the range 6 wt.% > W > 1.6 wt.%.

ACKNOWLEDGMENT

This research was supported in part by the U.S. Office of Naval Research under Project N00014-75-C-0541, and by the U.S. Air Force Materials Laboratory under contract No. F33615-71-C-1492.

REFERENCES

1. G. B. Belton and R. L. McCarron, *J. Phys. Chem.* **68**, 1852 (1964).
2. C. Wagner, *Corros. Sci.* **8**, 889 (1968).
3. W. W. Smeltzer and D. P. Whittle, *J. Electrochem. Soc.* **125**, 1116 (1978).
4. O. T. Ziebold and R. E. Ogilvie, *Anal. Chem.* **35**, 621 (1963).
5. S. Mrowec, "Attack of High Temperature Alloys in Sulfiding Gases," in *Properties of High Temperature Alloys*, Z. A. Foroulis and F. A. Pettit, eds. (Electrochem. Soc., Princeton, 1976).
6. G. C. Wood and T. Hodgkiess, *J. Electrochem. Soc.* **113**, 319 (1966).
7. C. S. Giggins and F. S. Pettit, *Trans. Met. Soc. A.I.M.E.* **245**, 2495 (1969).
8. G. C. Wood and T. Hodgkiess, *Nature* **211**, 1358 (1966).
9. G. H. Meier and R. A. Rapp, *Z. Phys. Chem.* **54**, 168 (1971).
10. C. E. Birchenall, "Diffusion in Oxides," in *Mass Transport in Oxides*, NBS Spec. Publ. 296, J. B. Wachtman and A. D. Franklin, eds. (1967), p. 119.
11. N. N. Khoi, W. W. Smeltzer, and J. D. Embury, *J. Electrochem. Soc.* **122**, 1495 (1975).
12. C. Wagner, *J. Electrochem. Soc.* **103**, 571 (1956).
13. S. Espevik, R. A. Rapp, P. L. Daniel, and J. P. Hirth, *Oxid. Met.* to be published.
14. L. C. Walters and R. E. Grace, *J. Appl. Phys.* **8**, 2331 (1968).
15. W. C. Hagel and A. U. Seybolt, *J. Electrochem. Soc.* **108**, 1146 (1961).
16. D. Caplan and G. I. Sproule, *Oxid. Met.* **9**, 459 (1975).
17. C. E. Birchenall, unpublished research, private communication.
18. K. Momma, H. Suto, and H. Oikawa, *Nippon Kinzoku Gakkaishi* **28**, 197 (1964).